

---

# The effect of scaffold architecture on properties of direct 3D fiber deposition of porous Ti6Al4V for orthopedic implants

---

J. P. Li,<sup>1,2</sup> J. R. de Wijn,<sup>1</sup> C. A. van Blitterswijk,<sup>1</sup> K. de Groot<sup>1,3</sup>

<sup>1</sup>Institute for Biomedical Technology, University of Twente, 7500 AE, Enschede, The Netherlands

<sup>2</sup>Porogen, B.V, 3723 MB, Bilthoven, The Netherlands

<sup>3</sup>CAM Implants, B.V, 2333 CL, Leiden, The Netherlands

Received 29 November 2006; revised 1 November 2007; accepted 25 July 2008

Published online 22 January 2009 in Wiley InterScience (www.interscience.wiley.com). DOI: 10.1002/jbm.a.32330

**Abstract:** 3D porous Ti6Al4V scaffolds were directly fabricated by a rapid prototyping technology, 3D fiber deposition (3DF). In this study, scaffolds with different structures were fabricated by changing fiber spacing and fiber orientation. The influence of different architectures on mechanical properties and permeability of the scaffold were investigated. Mechanical analysis revealed that compressive strength and E-modulus increase with decreasing the porosity. Permeability measurements showed that not only the total porosity but also the porous structure can influence the permeability. 3DF was found to provide

good control and reproducibility of the desired degree of porosity and the 3D structure. Results of this study demonstrate that the 3DF of Ti6Al4V give us flexibility and versatility to fabricate and improve scaffolds to better mimic the architecture and properties of natural bone and meet the requirements of bone graft substitutes and orthopedic and dental implants. © 2009 Wiley Periodicals, Inc. *J Biomed Mater Res* 92A: 33–42, 2010

**Key words:** porous Ti6Al4V; porosity; mechanical properties; scaffolds; 3D fiber deposition

---

## INTRODUCTION

At present, we are evaluating a porous Ti6Al4V to act as a scaffold for tissue engineering scaffold and orthopedic implants, which can, subsequently, be implanted in a bone defect for load bearing sites. Investigators have identified that porous scaffolds for such applications should have the following characteristics<sup>1–6</sup>: (1) A 3D, highly porous, and interconnected pore network, enabling cells to enter, attach, and migrate through the scaffold; (2) biocompatibility; (3) suitable surface structure and chemistry for cell attachment, proliferation, and differentiation; (4) mechanical properties to match those of the tissues at the site of implantation; and (5) easy to make into a variety of shapes and sizes with control of porous structure. Recently, it has also been shown that mismatches in geometry and mechanical stiffness of repair tissue as compared with the surrounding native tissues causes large stress levels, which may accelerate further joint degeneration.<sup>7,8</sup>

During the last 30 years, different processing techniques have been developed to make porous titanium and Ti alloys to be used in dental and orthopedic applications. These conventional techniques include sintering together of particles or plasma spraying of powder,<sup>9</sup> pressing and sintering of Ti fibers,<sup>10,11</sup> mixing powders with space-holder,<sup>12,13</sup> solid-state foaming by expansion of argon-filled pores,<sup>14</sup> and polymeric sponge replication.<sup>15</sup> Unfortunately, all of these processes form structures with randomly arranged pores with a wide variety of sizes and offer limited flexibility to control pore volumes and porosity distribution in the final structure. With such scaffolds, it is difficult to achieve the requirements of (5), and none of these conventional techniques enabled the production of scaffolds with a completely interconnected pore network. Not only the internal structure but also the external shape of implants should be tailored according to customer requirements. The imperfection of the conventional techniques has encouraged the use of a rapid prototyping (RP) technology.<sup>16</sup> RP, combining computer-aided design (CAD) with computer-aided manufacturing (CAM), which has the distinct advantage of enabling the building of objects with predefined microstructure and macrostructure, such as porosity,

Correspondence to: J. P. Li; e-mail: pingzi@excite.com

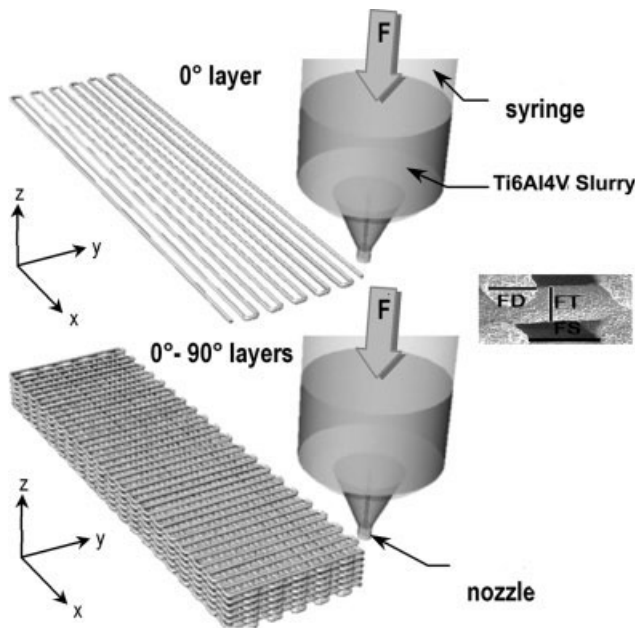


**Figure 1.** A schematic of a porous prototype made with 3D fiber deposition.

interconnectivity, and pore size. In the past, a few RP techniques were applied to make scaffolds, such as SLS (selective laser sintering),<sup>17,18</sup> SLM (selective laser melting),<sup>19</sup> EBM (electron beam melting),<sup>20,21</sup> and 3DP (3 dimension printing).<sup>22,23</sup> Until now most investigators focused on polymer and ceramic materials.<sup>17,23–27</sup> Recently, new 3D porous Ti6Al4V scaffolds were successfully developed in our group, which were directly fabricated by a RP technology, 3D fiber deposition (3DF). Figure 1 shows a schematic of a porous prototype made with 3DF deposition. 3DF, being a layer-by-layer manufacturing techniques, can be used to manufacture prototypes in which each layer may have a different fiber diameter (FD), thickness, fiber space (FS), and fiber orientation. It is similar as robotcasting patented by Cesarano et al of Sandia National Lab.<sup>28</sup> A brief comparison of these methods to produce porous scaffolds are summarized in Table I. In a previous study, the preparation of porous Ti6Al4V scaffolds and the optimization of processing parameters of 3DF deposition was discussed.<sup>29</sup> To meet practical requirements of bone ingrowth and long-term implantation, the porous structure of an implant was required to mimic the architecture and properties of natural bone, which will allow bone and tissue to grow into the pore spaces easily. Therefore, a mechanical and biological interlock between the implant and surrounding bone could be created.<sup>30</sup>

In this study, porous Ti6Al4V scaffolds with different structures were directly fabricated by changing fiber orientation and fiber spacing. Studies were conducted to investigate the influences of layer ori-

entation and fiber spacing on the porosity, the pore diameter, and the mechanical properties of various structures. These studies will determine the suitability of 3DF process for providing an effective and high degree of control over the sizes generated, and uniformity of their structure.

## MATERIALS AND METHODS

### Materials

Ti6Al4V powders (Bongen Titanium, China) with a mean diameter of 45  $\mu\text{m}$  and spherical shape were used in this study. A Ti6Al4V slurry was prepared as follows: The Ti6Al4V powders (68 vol %) were mixed with an aqueous solution of methylcellulose (0.3 wt %) as binder and stearic acid (0.2 wt %) to improve the rheological properties of the slurry.

### Processing parameters of 3D fiber deposition

Optimized 3DF process parameters were studied in a previous study. In this study, an inner nozzle diameter of 0.4 mm, a deposition pressure 2.5 bar, a feeding speed 350 mm/min, and an initial height between nozzle head and platform of 0.25 mm, were employed to fabricate different scaffolds for testing.

### Scaffold design and fabrication

Ti6Al4V scaffolds were fabricated for three experiments. The first experiment (Experiment I) is to investigate scaffolds with different internal structures. The second experiment (Experiment II) is to study the effect of structure and porosity on the scaffold mechanical properties. The third experiment (Experiment III) is to study the effect of structure and porosity on the permeability of scaffold as compared to that of human cancellous bone.

**TABLE I**  
Comparison of Different RP Techniques

	SLS	SLM	EBM	3DP	3DF
Speed	Low	Low	Fast	Low	Fast
Total time required	More	Less	Less	More	Less
Cost	Low	High	High	High	Low
Resolution	High	High	Low	High	Low
Anisotropic	No	No	No	No	Yes
Material needed for test	Less	More	More	More	Less
Material variety	More	More	More	Less	More
Surface quality	High	High	Low	High	High
Density	Low	Low	High	Low	Low
Dimension accuracy					
shrinkage	High	Low	Low	High	High
Support structure	Yes	Yes	Yes	Yes	No
Sintering	Yes	No	No	Yes	Yes
Removal of excess powder	Yes	Yes	Difficult	Yes	No

**TABLE II**  
**Scaffold Groups for Experiment**

Specimen Group	Nozzle Size (mm)	Lay-Down Pattern	Fiber Space (mm)	Layer Thickness (mm)
S1	0.4	[0/90]n	0.5	0.32
S2	0.4	[0/0/90/90]n	0.5	0.32
S3	0.4	[0/90]sn	0.5	0.32
S4	0.4	[0/45/90/135]n	0.5	0.32
P03	0.4	[0/90]sn	0.3	0.32
P04	0.4	[0/90]n	0.4	0.32
P05	0.4	[0/90]n	0.5	0.32
P06	0.4	[0/90]n	0.6	0.32
P07	0.4	[0/90]n	0.7	0.32
P08	0.4	[0/90]n	0.8	0.32

For the scaffolds with different structures, four kinds of models were designed and made with a fiber spacing of 0.5 mm, a FD of 0.4 mm, and layer thickness (LT) of 0.35 mm; four lay-down patterns of [0/90]n, [0/0/90/90]n, [0/45/90/135]n, and [0/90]sn (s represents staggered) (S1, S2, S3, and S4 corresponded to different structure).

For scaffolds with different porosity, a single design was used with variable fiber spacing (0.3, 0.4, 0.5, 0.6, 0.7, 0.8 mm, lay-down pattern: [0/90]n) (P03, P04, P05, P06, P07, and P08 in Table II).

For all experiments, a total of 50 blocks (three blocks, per condition) was produced. The block size is 22 mm × 22 mm × 10 mm.

### Sintering of scaffolds

After fiber deposition, the samples were first dried for at least 24 h at room temperature, then for 3 h at 80°C, and eventually sintered in a high vacuum furnace ( $10^{-5}$  mbar) with a heating profile as follows:

RT 600 min → 500°C 450 min → 1200°C 120 min  
→ 1200°C furnace colling → 25°C

### Preparation of samples for properties test

The porosity of the sintered blocks was calculated by measuring length, width, and height as described in the following section. After calculating the porosity, each block was machined by electrical discharge machining to obtain Ø7 mm by 9 mm cylinders for mechanical tests and permeability tests. The samples were labeled for two directions: the Z direction and X- or Y-directions with respect to the lay-down pattern of [0/90]n and [0/45]n. The structure in X- and Y-direction was considered to be the same.

### Characterization of scaffold

#### Porosity

Porosity ( $\rho$ ) was calculated by measuring the apparent density ( $\rho_b$  = weight of sample/volume of sample) and

using the formula:  $\rho = (1 - \rho_b/\rho_s) \times 100$ , where  $\rho_s$  is the density of 100% dense material (4.5 g/cm<sup>3</sup>). A total of five samples per structure were measured.

### Morphology

The scaffold morphology was studied with environmental scanning electron microscopy (ESEM, Model XL-30, Philips, Eindhoven, The Netherlands). The ESEM micrographs were used to measure the FS, FD, and LT besides studying the scaffold morphology. FS was defined as the edge-to-edge distance between two fibers. LT was defined as the edge-to-edge distance between two layers. FS and FD values were measured from layer views, which showed lay-down pattern. LT value was measured from the cross-section views of scaffold specimens, which showed the stacked layers. The dimensions FS, LT, and FD are illustrated in Figure 1.

### Mechanical test

Five samples from each kind of scaffold were randomly chosen. The compression tests of porous Ti6Al4V samples (Ø7 mm × 9 mm,  $n = 5$ ) were performed at room temperature with a crosshead speed of 1 mm/min (Zwick/Z050, Germany). The E-modulus was calculated by the load increment and the corresponding crosshead displacement between the points on the straight-line part. Because of the much higher stiffness of the load cell of the testing machine as compared to that of the sample, the increment of the crosshead displacement was assumed to be equal to the deformation of the sample.

### Permeability

A permeability test was performed with a self-designed permeability-meter.<sup>31</sup> Briefly, a cylindrical sample (Ø7 mm × 9 mm) was mounted in a tube connected to a wide diameter water reservoir which was positioned at a certain constant height. The flow of water through the sample was measured in mL/s. Normalized for the dimensions of the sample, it provided a measure for the sample's permeability. The samples with different structure and porosity were tested to study the relationship between permeability and structure or porosity. Two samples under Z-direction of each condition were tested.

### Statistical analysis

The statistical significance was determined by a *t*-test at the significance level of  $p < 0.05$

### Acetabular cup design and fabrication

The 3DF fabrication technique was successfully used to build acetabular cup scaffolds designed with image-based design techniques. In briefly, a cup with a diameter of 50 mm and a wall thickness of 5 mm was designed using Rhinoceros software 3D [Fig. 8(A)], then the dataset of the

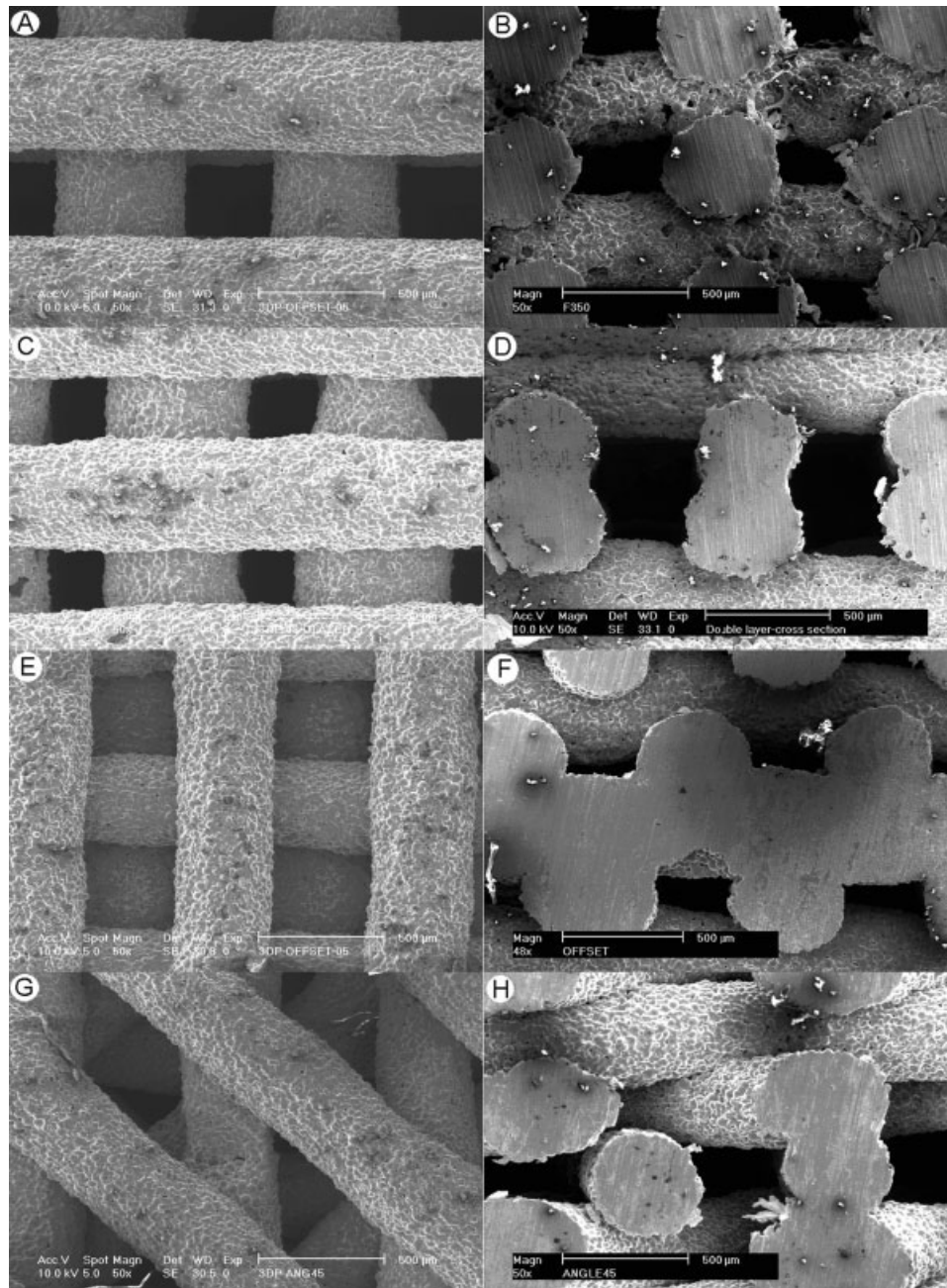


**Figure 2.** Scaffold with different lay-down patterns. A) Lay-down patterns of  $[0/90]_n$ . B) Lay-down pattern of  $[0/0/90/90]_n$ . C) Lay-down pattern of  $[0/90]_{sn}$  (s represents staggered). D) Lay-down pattern of  $[0/45/90/135]_n$ .

cup was transported to a 3D biplotter. The FS was set to 500  $\mu\text{m}$ ; the LT is 320  $\mu\text{m}$ , resulting pore size of cup [Fig. 8(B,C)] around 400  $\mu\text{m}$ . It can be seen that resulting acetabular cup replicated the design very well.

## RESULTS

### Morphology

Figure 2 shows the scaffolds with different structures. It can be seen that the scaffold has two pat-

terns under Z-direction view. One group with square pores as a result of  $[0/90]_n$  lay-down pattern [Fig. 2(A-F)], and the other with triangular pores as a result of a  $[0/45]_n$  lay-down pattern [Fig. 2(G,H)]. When the scaffolds are viewed in the X- or Y-direction of the fabrication process, more differences between the four scaffolds become overt.

Figure 3 shows a series of surface morphologies of scaffolds built with varying fiber spacing from 0.2 to 0.7 mm in increments of 0.1 mm at constant LT and FD of 0.32 and 0.4 mm, respectively. It can be seen

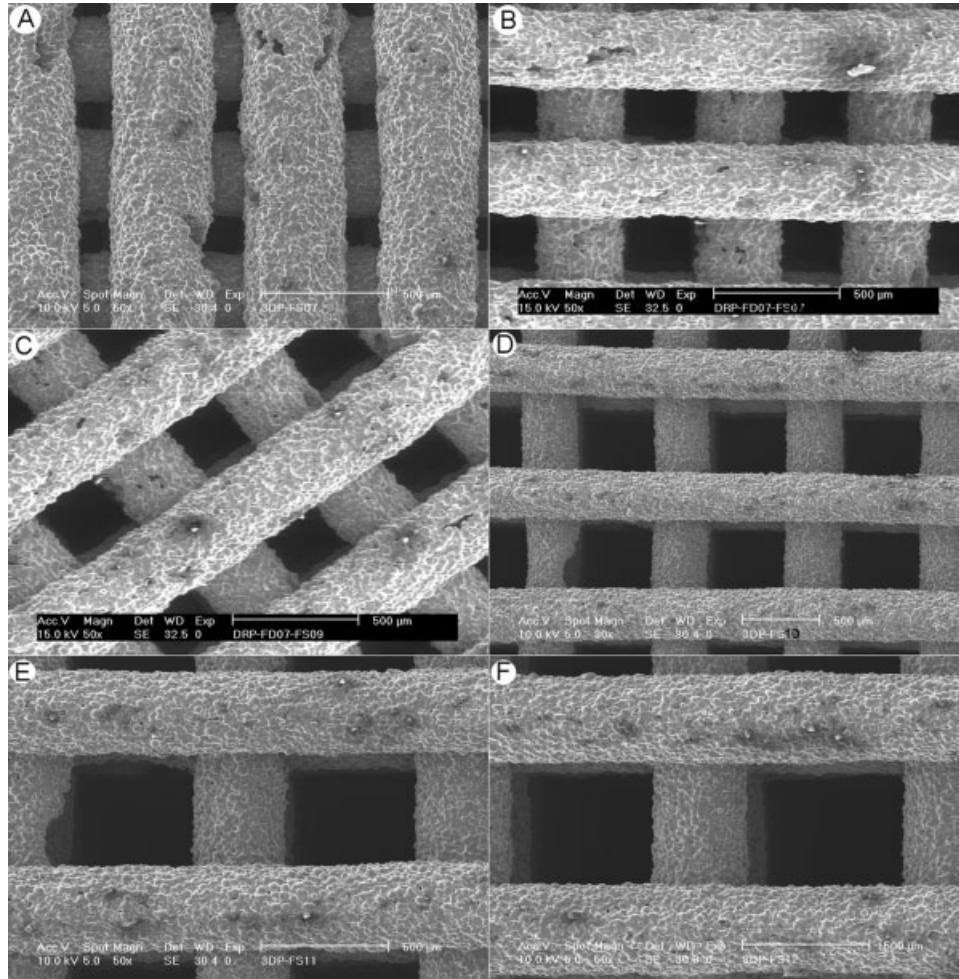


**Figure 3.** Scaffold with different fiber spacing. A) FS02, B) FS03, C) FS04, D) FS05, E) FS06, F) FS07.

that with decreasing the FS the structure becomes denser and the porosity decreases.

Based on the ESEM measurement, features of scaffold made by 3DF are shown in Table III. It can be seen that by changing the lay-down pattern and the FS, scaffolds with different pore structure and porosity are obtained. Because of sintering at a tempera-

ture of 1200°C, some shrinkage has to be expected as a result of necking of the particles. It can be found in the Table II, when compared to the machine settings (Table I), that the shrinkage in the scaffolds is apparently not homogenous and ranges from a few percentage to sometimes 20%. The FD is near to the inner size of nozzle, but the fiber spacing (FS)

**TABLE III**  
Measurement of Structural Features of Ti6Al4V Scaffold

Specimen Group	Fiber Diameter (μm)	Shrinkage of Fiber (%)	Fiber Space (μm)	Layer Thickness (μm)	Shrinkage of LT (%)	Porosity (%)
S1	369 ± 12	7.7	381 ± 15	301 ± 20	5.9	54.5 ± 3.5
S2	388 ± 16	3	394 ± 18	282 ± 21	11.8	53.5 ± 2.2
S3	370 ± 16	7.7	402 ± 7	302 ± 28	5.6	53 ± 2.1
S4	388 ± 25	3	405 ± 17	293 ± 15	8.4	55 ± 1.4
P03	368 ± 22	8	160 ± 34	275 ± 24	14	39 ± 2.1
P04	375 ± 17	6.2	261 ± 26	286 ± 17	10.6	45 ± 2.8
P05	355 ± 10	11	396 ± 16	263 ± 29	17.8	54 ± 2.2
P06	365 ± 18	8.7	465 ± 7	277 ± 27	13.4	58 ± 1.4
P07	385 ± 14	3.7	556 ± 12	258 ± 32	19.3	62 ± 0.7
P08	381 ± 7	4.7	679 ± 10	301 ± 14	5.9	70 ± 1

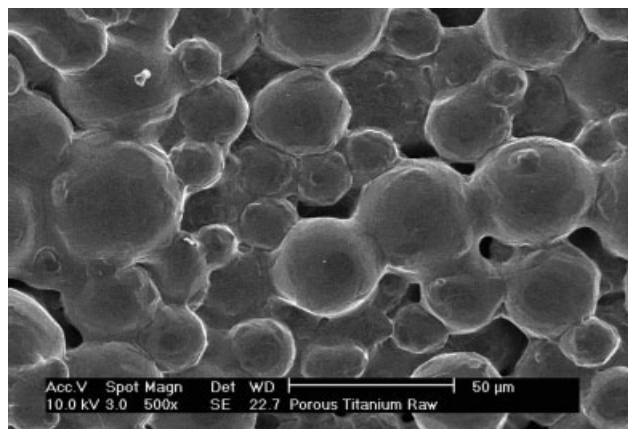


**Figure 4.** High magnification of fiber surface.

changes significantly. Measurements of FS and fiber thickness (FT) showed that the pore size ranges between 160 to 680  $\mu\text{m}$  (horizontal) and 300  $\mu\text{m}$  (vertical).

### Porosity

The porosity of the scaffold showed little variation. Scaffolds made by different lay-down patterns have similar porosity when the settings for FD, FS, and LT are the same (Table II). Actually, this porosity consists of macroporosity and microporosity. Macroporosity results from fiber spacing and fiber thickness. Microporosity results from necking of the particles during powder sintering and residual gas in the starting titanium slurry. High magnification of fiber surface proves this (Fig. 4).

### Mechanical properties

The mechanical properties of scaffolds were evaluated by measuring the compressive strength and the E-modulus.

#### Compressive strength

The average values of compressive strength of different scaffolds are plotted against structure and FS setting, as shown in Figure 5. Figure 5(A) shows the compressive strength of scaffold with different structure in Z-direction and X- or Y-direction. Scaffolds with a [0/90] $n$  and [0/45/90/135] $n$  lay-down pattern had a higher compressive strength in the Z-direction as compared to other patterns. In the X- or Y-direction scaffolds with a [0/90] $n$  lay-down pattern had the highest compressive strength. Figure 5(B) shows the compressive strength of scaffolds with different FS in Z-direction and X- or Y-direction. The com-

pressive strength decreases with increasing FS. This is due to the decrease of the number of fibers within each layer, resulting in a decrease of the amount of loading area. In other words, the compressive strength of porous scaffolds depends on the porosity or relative density. There is no significant difference between the compressive strength of scaffolds with [0/90] $n$  lay-down pattern in Z-direction and in X- or Y-directions. Only with [0/45] patterns significant differences ( $p < 0.05$ ) of the compressive strength under two directions are found.

#### E-modulus

The calculated E-modulus of different scaffolds was shown in Figure 6(A,B). Figure 6(A) shows the E-modulus of scaffold with different structure under Z-direction and X- or Y-direction. Scaffolds with a 0/45° lay-down pattern had the lowest E-modulus in two directions as compared to other scaffolds, and scaffolds with different lay-down pattern showed little variation of E-modulus under Z-direction. However, there is a significant difference again between

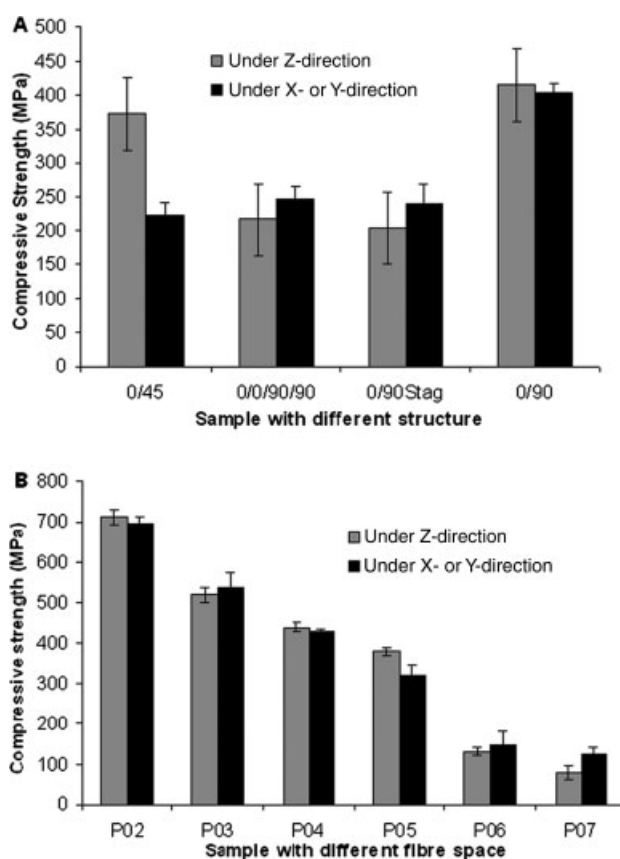


**Figure 5.** Comparison of compressive strength under Z-direction and X- or Y- direction. A) Scaffold with different structure (fiber spacing: 500  $\mu\text{m}$ , porosity: 55%); B) Scaffolds with different porosity (lay-down pattern: 0/90).

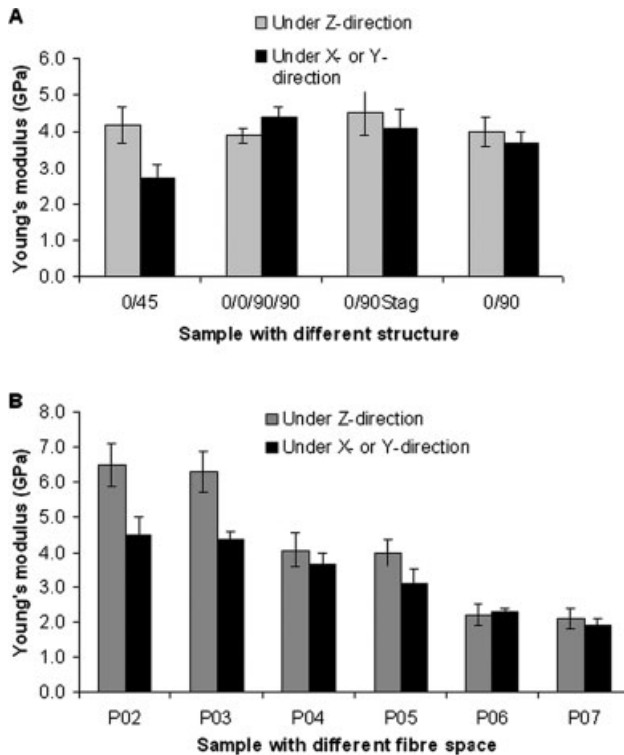


**Figure 6.** Comparison of Young's modulus under Z-direction and X- or Y-direction. A) Scaffolds with different structure (fiber spacing: 500  $\mu\text{m}$ , porosity: 55%); B) Scaffolds with different porosity (lay pattern: [0/90]).

the E-modulus of scaffolds with 0/45° lay-down pattern in Z-direction and in X- or Y-direction. Figure 6(B) shows the E-modulus of scaffolds with different FS in Z-direction and X- or Y-direction. It can also be seen that the E-modulus of different scaffolds decrease with increasing FS. There is significant difference ( $p < 0.05$ ) in two directions while FS is below P04 but no such evidence was seen with FS above P05.

### Permeability

Figure 7 shows the permeability data in the Z direction of porous Ti6Al4V with different structures and porosities as compared with human cancellous bone under transverse direction.<sup>32</sup> It is clear that the pore structure affects the permeability of scaffold. At left part of Figure 7, scaffolds with different structure have the same porosity, but different permeability. At right part, scaffolds with different porosity and same structure, resulted in different permeability. The permeability of scaffolds with lay-down patterns [0/45] and [0/90] as measured in the Z-direction is similar to that of human cancellous bone. The porosity of human cancellous bone is around 60%. It can be seen that the porosity affected

the permeability greatly. Moreover, the permeability test enables us to prove repeatability of the 3DF process under same parameters. In one batch of samples, the standard deviation in permeability is relatively low. The measured porosities (listed in Table II) also prove the repeatability of this process.

### Acetabular cup design and fabrication

The 3DF fabrication technique was used successfully to build acetabular cup scaffolds designed using image-based design techniques. Briefly, a cup with a diameter of 50 mm and a wall thickness of 5 mm was designed using Rhinoceros software 3D [Fig. 8(A)], then the dataset of cup was transported to a 3D bioplotter. The FS was set to 500  $\mu\text{m}$ ; the LT is 320  $\mu\text{m}$ , resulting pore size of cup [Fig. 8(B,C)] around 400  $\mu\text{m}$ . It can be seen that resulting acetabular cup replicated the design well. The total porosity of the cup is around 55%. The dimensions of green body are 50 mm in diameter and 25 mm in height, after sintering, the dimensions are 46.3 and 21.8 mm, respectively.

## DISCUSSION

The results show that the fiber spacing (FS) played an important role in the porosity for each scaffold. Since a pore is the space created between successive strands within a layer, the pore formed in the scaffold increases in size by increasing the value of FS. However, this value cannot be increased indefinitely as slacking will occur when there is insufficient strength for an extruded fiber to bridge a gap.<sup>27,33,34</sup> Generally, the gap of below 10 mm could be bridged by this slurry. It was essential that every layer is well deposited as the preceding layer served as the foundation for the next layer. In the previous study, the parameters of 3DF effect on the porosity of scaffold

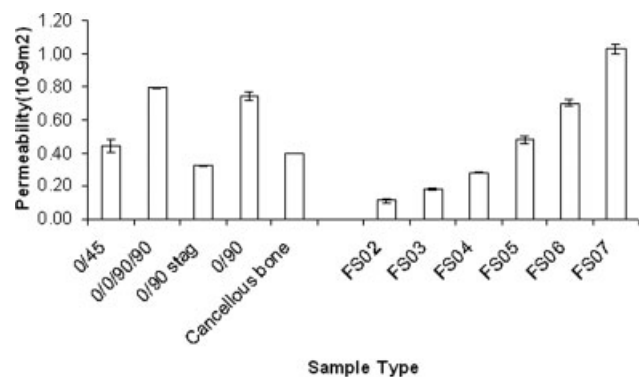


**Figure 7.** Permeability as function of different structure and porosity compared with that of cancellous bone.

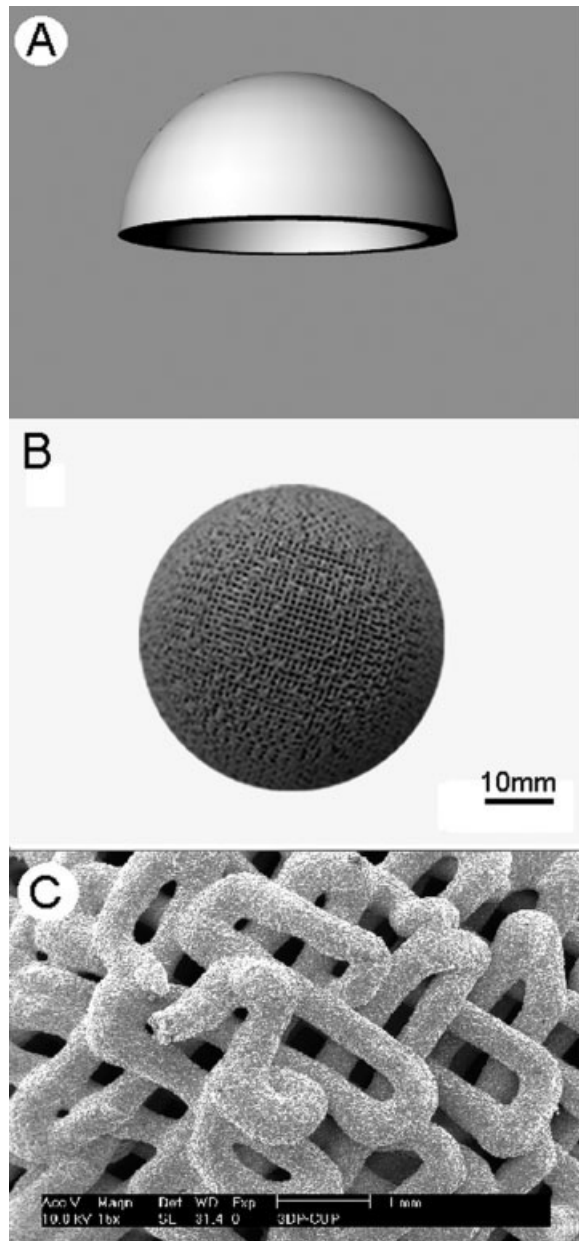


**Figure 8.** Prototype of acetabular cup. A) Image design by CAD software, B) Porous acetabular cup by 3DF, C) High magnification of acetabular cup surface.

fold, especially feeding speed and air pressure on the slurry, were described. However, increasing speed to stretch the extruded fiber or changing pressure to reduce the amount of Ti slurry might affect the stability of the scaffold and reproducibility.

The flexibility of 3DF for changing the FS setting allows highly consistent, controllable, and reproducible pore size and arrangement. In this study, FS was set from 200 to 800  $\mu\text{m}$ , resulting in pore sizes ranging from 160 to 680  $\mu\text{m}$ , meeting the requirements for bony ingrowth.<sup>35,36</sup>

When scaffolds were viewed in the Z-direction and the X- or Y-direction, the 3D interconnectivity of

pores was observed to be as in Figures 2 and 3, not unlike to the bee's honeycomb with a regular array. It reveals that 3DF is capable of producing a matrix-like structure or scaffold that is consistently controllable, with reproducible porosity and uniform pore arrangement. The consistency and repeatability of the extruded fibers, fiber arrangement, and FS setting enables the production of matrix-like structures with intended and predictable macrostructure. These conditions are highly favorable, since they allow the user to predict accurately and produce structures with known pore sizes and arrangement.

Apparently, by increasing the number of layer with different fiber orientation in a multilayered scaffold, it is possible to make a porous 3D scaffold with various degrees of channel dimensions. Meanwhile, the use of a finer nozzle diameter allow the fabrication of scaffolds with finer architecture, and a higher surface area to volume ratio can be obtained compared with the scaffold made by a big nozzle.<sup>27</sup>

When compressed under Z-direction, it is the fiber joints of adjacent layers that bear the loading force. It is clear that a larger number of fiber joints per unit area would be expected to strengthen the scaffold structure. When scaffolds are compressed under X- or Y-direction, it is the axial fiber that bears the loading strength. In this case, the compressive strength is dependent on the number of fibers per unit area aligned in the loading direction and the angles of lay-down pattern. Our results of changing FS and lay-down pattern prove this. The strength of a scaffold is expected to be higher when compressed in the direction with a higher degree of fiber alignment as compared to the case of a  $[0/45]_n$  lay-down pattern.

Although ceramics are good bone substitutes (osteoconductive), they do not provide sufficient strength for load-bearing conditions. Ti6Al4V scaffolds made by 3DF have a compressive strengths ranging from 110 to 650 MPa with porosities ranging from 70 to 30%. The compressive strength is higher than that of cancellous bone and comparable to that of cortical bone.<sup>37</sup> It is known that implants with high elastic moduli offer the risk of stress shielding, which lead to bone resorption and eventual loosening of the implant.<sup>38–40</sup> Although dense Ti6Al4V has a Young's modulus only about half of those of 316L stainless steel or CoCrMo alloy,<sup>41,42</sup> it is still about 10–20 times higher than the E-modulus of human bone. The E-moduli of 3DF scaffolds with porosities of 39–70% ranged from 1.9 to 4.5GPa, which is between that of cancellous bone and cortical bone.<sup>41,42</sup>

The permeability of scaffolds with  $0/45^\circ$  and  $0/90^\circ$  and staggered lay-down patterns is quite comparable to that of human cancellous bone. Therefore such scaffolds are promising biomaterials for biomedical applications, since a higher metabolic exchange rate of bone cells as well as minerals can

be achieved by its interconnected pore structure and a high surface to volume ratio. High permeability could also be highly beneficial for cell seeding and tissue formation since it allows the cells to diffuse into the center of the scaffold and provide more space for the ingrowth of tissue and subsequent vascularization. Therefore, the osteoconductive potential<sup>43,44</sup> of the material maybe increased.

Permeability data reflect a combination of (1) porosity, (2) pore size and distribution, (3) interconnectivity, (4) interconnection pore size and distribution, (5) orientation of pores with respect to flow direction. Therefore, in the future, permeability can be taken as an intrinsic parameter for describing macroporous structures, probably with more relevancy than porosity and mean pore size.

It can be seen that there are several advantages of this type of scaffolds. First, the structure of the scaffold is highly regular and repeatable and all pores are interconnective. Secondly, scaffolds with regular architecture could make the seeding of cells up to the core easier than in random architecture scaffolds and an environment, which encourages uniform conditions for free of flowing nutrients to the interior of implant and promoting cell viability, will be created. Finally, regular architecture scaffolds could permit parametric analyses to be conducted in terms of nutrient concentration and local environments. It is essential in scientific investigations to identify and predict optimal cell environments and to know how scaffolds and material affect tissue regeneration.

## CONCLUSION

3DF was successfully applied to fabricate porous Ti6Al4V scaffolds with fully interconnected pore networks, highly controllable porosities, and pore sizes. These scaffolds can be made with different structures and porosities by controlling of process parameters such as fiber spacing, LT, and fiber orientation. The characteristic of the resulting scaffold were analyzed. Experimental results show that the fiber spacing has a profound effect on the porosity, pore size, compressive strength, and elastic modulus of the scaffolds. The resulting scaffolds can mimic the properties of both the cancellous bone and the cortical bone. This technique also provides a control of external shape to match graft geometry and internal architecture while the pore structure in 3D space provides control over interconnectivity, geometry, FD, and orientation and mechanical properties. Therefore, 3DF is a promising new technique for design and fabrication of tailor-made or custom-made Ti6Al4V scaffold architectures for orthopedic implant applications.

## References

1. Yang S, Leong KF, Du Z, Chua CK. The design of scaffolds for use in tissue engineering, Part 1: Traditional factors. *Tissue Eng* 2001;7:679–689.
2. Vacanti JP, Vacanti CA. The history and scope of tissue engineering. In: Lanza RP, Langer R, Chick WL, editors. *Principles of Tissue Engineering*, 2nd ed. New York: Academic Press; 2000. p 3–8.
3. Hollister S, Lin C, Saito E, Schek R, Taboas J, Williams J, Partee B, Flanagan C, Diggs A, Wilke E, Van Lenthe GH, Müller R, Wirtz T, Das S, Feinberg SE, Krebsbach PH. Engineering craniofacial scaffolds. *Orthod Craniofac Res* 2005;8:162–173.
4. Hutmacher DW, Schantz T, Zein I, Ng KW, Teoh SH, Tan KC. Mechanical properties and cell cultural response of polycaprolactone scaffolds designed and fabricated via fused deposition modeling. *J Biomed Mater Res* 2001;55:203–216.
5. Hutmacher DW. Scaffold design and fabrication technologies for engineering tissues—State of the art and future perspectives. *J Biomater Sci Polym Ed* 2001;12:107–124.
6. Hutmacher DW. Scaffolds in tissue engineering bone and cartilage. *Biomaterials* 2000;21:2529–2543.
7. Pompe W, Worch H, Epple M, Friess W, Gelinsky M, Greil P, Hempele U, Scharnweber D, Schulte K. Functionally graded materials for biomedical applications. *Mater Sci Eng A* 2003;362:40–60.
8. McNamara BP, Cristofolini L, Toni A, Taylor D. Relationship between bone prosthesis bonding and load transfer in total hip reconstruction. *J Biomech* 1997;30:621–630.
9. Fujibayashi S, Neo M, Kim HM, Kokubo T, Nakamura T. Osteoinduction of porous bioactive titanium metal. *Biomaterials* 2004;25:443–450.
10. Galante J, Rostoker W. Fiber metal composites in the fixation of skeletal prosthesis. *J Biomed Mater Res* 1973;4:43–61.
11. Galante J, Rostoker W, Lueck R, Ray RD. Sintered fiber metal composites as a basis for attachment of implants to bone. *J Bone Joint Surg Am* 1971;53:101–114.
12. Wen C, Yamata Y, Mabuchi M. Processing and mechanical properties of autogenous titanium implant materials. *J Mater Sci Mater Med* 2002;13:397–401.
13. Matin B, Cornelia S, Bronkremer HP, Baur H. High-porosity titanium, stainless steel, and superalloy parts. *Adv Eng Mater* 2000;2:196–199.
14. Davis NG, Teisen J, Schuh C, Dunand DC. Solid-state foaming of titanium by superplastic expansion of argon-filled pores. *J Mater Res* 2001;16:1508–1539.
15. Li JP, Li SH, Van Blitterswijk CA, De Groot K. A novel porous Ti6Al4V: Characterization and cell attachment. *J Biomed Mater Res* 2005;73A:223–233.
16. Yang S, Leong KF, Du Z, Chua CK. The design of scaffolds for use in tissue engineering, Part 2: Rapid prototyping techniques. *Tissue Eng* 2002;8:1–11.
17. Chua CK, Leong KF, Tan KH, Wiria FE, Cheah CM. Development of tissue scaffolds using selective laser sintering of polyvinyl alcohol/hydroxyapatite biocomposite for craniofacial and joint defects. *J Mater Sci Mater Med* 2004;15:1113–1121.
18. Bill JS, Reuther JF. Rapid prototyping in planning reconstructive surgery of the head and neck. Review and evaluation of indications in clinical use. *Mund Kiefer Gesichtschir* 2004;8:135–153.
19. Lin CY, Wirtz T, Lamarca F, Hollister SJ. Structural and mechanical evaluations of a topology optimized titanium interbody fusion cage fabricated by selective laser melting process. *J Biomed Mater Res A* 2007;83:272–279.
20. Hollander DA, von Walter M, Wirtz T, Sellei R, Schmidt-Rohlfing B, Paar O, Erli HJ. Structural, mechanical and in vitro characterization of individually structured Ti-6Al-4V

- produced by direct laser forming. *Biomaterials* 2006;27:955–963.
21. Harrysson OL, Hosni YA, Nayfeh JF. Custom-designed orthopedic implants evaluated using finite element analysis of patient-specific computed tomography data: Femoral-component case study. *BMC Musculoskelet Disord* 2007;8:91.
  22. Curodeau A, Sachs E, Caldarise S. Design and fabrication of cast orthopedic implants with freeform surface textures from 3-D printed ceramic shell. *J Biomed Mater Res* 2000;53:525–535.
  23. Seitz H, Rieder W, Irsen S, Leukers B, Tille C. Three-dimensional printing of porous ceramic scaffolds for bone tissue engineering. *J Biomed Mater Res B Appl Biomater* 2005;74:782–788.
  24. Tan KH, Chua CK, Leong KF, Naing MW, Cheah CM. Fabrication and characterization of three-dimensional poly(ether-ether-ketone)/-hydroxyapatite biocomposite scaffolds using laser sintering. *Proc Inst Mech Eng [H]* 2005;219:183–194.
  25. Dhariwala B, Hunt E, Boland T. Rapid prototyping of tissue-engineering constructs, using photopolymerizable hydrogels and stereolithography. *Tissue Eng* 2004;10:1316–1322.
  26. Wilson CE, de Bruijn JD, van Blitterswijk CA, Verbout AJ, Dhert WJ. Design and fabrication of standardized hydroxyapatite scaffolds with a defined macro-architecture by rapid prototyping for bone-tissue-engineering research. *J Biomed Mater Res A* 2004;68:123–132.
  27. Zein I, Huttmacher DW, Tan KC, Teoh SH. Fused deposition modeling of novel scaffold architectures for tissue engineering applications. *Biomaterials* 2002;23:1169–1185.
  28. Dellinger JG, Cesarano J III, Jamison RD. Robotic deposition of model hydroxyapatite scaffolds with multiple architectures and multiscale porosity for bone tissue engineering. *J Biomed Mater Res A* 2007;82:383–394.
  29. Datta N, Holtorf HL, Sikavitsas VI, Jansen JA, Mikos AG. Effect of bone extracellular matrix synthesized in vitro on the osteoblastic differentiation of marrow stromal cells. *Biomaterials* 2005;26:971–977.
  30. Sun W, Starly B, Nam J, Darling A. Bio-CAD modeling and its applications in computer-aided tissue engineering. *Comput Aided Des* 2005;37:1097–1114.
  31. Li SH, De Wijn JR, Li JP, Layrolle P. Biphasic calcium phosphate scaffold with high permeability/porosity ratio. *Tissue Eng* 2003;9:535–548.
  32. Grimm MJ, Williams JL. Measurement of permeability in human calcaneal trabecular bone. *J Biomech* 1997;30:743–745.
  33. Landers R, Mulhaupt R. Desktop manufacturing of complex objects, prototypes and biomedical scaffolds by means of computer-assisted design combined with computer-guided 3D plotting of polymers and reactive oligomers. *Macromol Mater Eng* 2000;282:17–21.
  34. Landers R, Pfister A, John H, Hubner U, Schmelzeisen R, Mulhaupt R. Fabrication of soft tissue engineering scaffolds by means of rapid prototyping techniques. *J Mater Sci* 2002;37:3107–3116.
  35. Pilliar RM. P/M processing of surgical implants: Sintered porous surfaces for tissue-to-implant fixation. *Int J Powder Metall* 1998;34:33–45.
  36. Pilliar RM. Porous-surfaced metallic implants for orthopedic applications. *J Biomed Mater Res* 1987;21(A1 Suppl):1–33.
  37. Li JP, Li SH, Van Blitterswijk CA, de Groot K. Cancellous bone from porous Ti6Al4V by multiple coating technique. *J Mater Sci Mater Med* 2006;17:179–185.
  38. Cheal E, Spector M, Hayes W. Role of loads and prosthesis material properties on the mechanics of the proximal femur after total hip arthroplasty. *J Orthop Res* 1992;10:405–422.
  39. Prendergast P, Taylor D. Stress analysis of the proximo-medial femur after total hip replacement. *J Biomed Eng* 1990;12:379–382.
  40. Lewis JL, Askew MJ, Wixson RL, Kramer GM, Tarr RR. The influence of prosthetic stem stiffness and of a calcar collar on stresses in the proximal end of the femur with a cemented femoral component. *J Bone Joint Surg Am* 1984;66:280–286.
  41. Bobynd JD, Hacking SA, Chan SP. Characterization of a new porous tantalum biomaterial for reconstructive orthopaedics. In: Scientific Exhibit, Proceedings of AAOS, Anaheim, CA, 1999.
  42. Krygier JJ, Bobynd JD, Poggie RA. Mechanical characterization of a new porous tantalum biomaterial for orthopaedic reconstruction. In: Proceedings of SIROT, Sydney, Australia, 1999.
  43. Hui PW, Leung PC, Sher A. Fluid conductance of cancellous bone graft as a predictor for graft-host interface healing. *J Biomech* 1996;29:123–132.
  44. Shimko DA, Shimko VF, Sander EA, Dickson KF, Nauman EA. Effect of porosity on the fluid flow characteristics and mechanical properties of tantalum scaffolds. *J Biomed Mater Res B Appl Biomater* 2005;73:315–324.